Available online at www.sciencedirect.com
SCIENCE DIRECT®
Journal of Nuclear Materials 350 (2006) 271–283
journal of nuclear materials
www.elsevier.com/locate/jnucmat

A model for the behavior of thorium uranium mixed oxide kernels in the pelletizing process

R.A.N. Ferreira [a,*], E. Jordão [b]

[a] Centro de Desenvolvimento da Tecnologia Nuclear – CDTN/CNEN CP 941, 30 123–970, Belo Horizonte, Brazil
[b] Universidade Estadual de Campinas – UNICAMP/FEQ CP 8 066, 13 084–970, Campinas, Brazil

Received 12 April 2005; accepted 27 December 2005

Abstract

A behavior model of nuclear fuel kernels in the pelletizing process was developed to predict the microstructure of (Th,5%U)O_2 sintered pellets. Methods, equipments and components were developed in order to measure the density, the specific surface area and the crushing strength of the kernels and produce fuel pellets. It enables a correlation between the kernels properties and the microstructure, density and open porosity that were obtained in the fuel pellet produced with these kernels. It was possible to obtain a mathematical expression that allows one to calculate, from the kernel density and specific surface, the density that will be obtained in the fuel pellet for each compactation pressure value. The investigation showed which kernels properties are desired to obtain fuel pellets that satisfy the quality requirements for a stable performance in a power reactor. This model has been validated by experimental results and fuel pellets were obtained with an optimized microstructure that satisfies the fuel specification for an in-pile stable behavior.

PACS: 28.41.B; 81.20.Ev; 81.20.Fw

1. Introduction

To demonstrate the possibility of thorium utilization in pressurized water reactors, a research program was carried out with a cooperative work between Germany and Brazil [1,2]. In this program, a process to measure the crushing strength of (Th,U)O_2 kernels was developed in order to study the behavior of an isolated kernel in a compression test. The aim was finding the dependence between the isolated behavior and the behavior of thousands of these kernels conjunctly under pressure in the pelletizing process and so to elaborate a behavior model that helps the development of the new fuel and the optimization of its microstructure. A mathematical expression was obtained for the sintered pellet density (ρ_s) as a function of the compactation pressure (P_c) and the raw material properties, crushing strength (F_c), density (ρ_m), and specific surface (S_g), i.e., a mathematical expression for the following equation:

$$\rho_s = \rho_s(F_c, \rho_m, S_g, P_c). \quad (1)$$

* Corresponding author. Tel.: +55 31 3499 3150.
E-mail address: ranf@cdtn.br (R.A.N. Ferreira).

0022-3115/$ - see front matter © 2006 Elsevier B.V. All rights reserved.
doi:10.1016/j.jnucmat.2005.12.006

This model is based on the degree of the voids decreasing between the kernels during pressing, and shows the mechanisms that define the behavior of the material and which material properties are interrelated with the fuel pellet properties, such as microstructure, density and open porosity.

2. Experimental procedures

2.1. Kernels production – sol–gel process [3,4]

For the kernels production, aqueous solutions of uranyl nitrate and thorium nitrate are homogeneously mixed in a specified ratio. To this feed solution, it is added polyvinyl alcohol (PVA) as an auxiliary material to increase the solution viscosity and carbon black as pore former to lowering the mechanical strength of the kernels in order to make easier their desintegration during pressing. Finally, to avoid agglomeration of the carbon black that can cause obstruction of the equipment nozzle, tetrahydrofurfuryl alcohol (THFA) or ethanol is added to the feed solution. Using mechanical vibration of an electromagnetic vibration system, this feed solution passes through nozzles, generating jets of liquid in the air which are dispersed into uniform kernels. Their surfaces are hardened by chemical reaction with ammonia gas before being collected in an ammonia aqueous solution where the external gelation reaction is fulfilled (Fig. 1). Subsequently, the kernels are washed with water in order to eliminate the reaction by-product ammonium nitrate. Drying and calcining are performed in the air. Thus, the thorium hydrate is dehydrated, the ammonium diuranate and the PVA are thermally decomposed and the carbon black is burnt, leaving pressing pores in the microstructure of the kernels.

2.2. Fuel pellets fabrication

For the fabrication of the $(Th,U)O_2$ pellets, a compactation system was developed at CDTN to be mounted in a special model of hydraulic press manufactured under request by Angelo Ciola and Filhos from modifications in the standard model of the type 'C' hydraulic press shown in Fig. 2 [5].

The lower punch is fixed but the die can fluctuate. The die movement is adjustable and it is lubrificated using Petrobrás CL-OF-130 oil. The oil is injected, under pressure, through the lower punch when the die moves back to the charging position. For an upper punch diameter of 1.108 cm, the maximal capacity of the equipment is 1200 MPa and it can work with double effect through the fluctuation of the die in order to obtain a symmetrical density gradient along the pellet.

The pellets sintering was performed in an oven furnish by Astro Industries and Co., CA, USA. It has a platinum/50%rhodium heating element that can operate in air. The sinterings were performed inside an alumina tube under controlled atmosphere

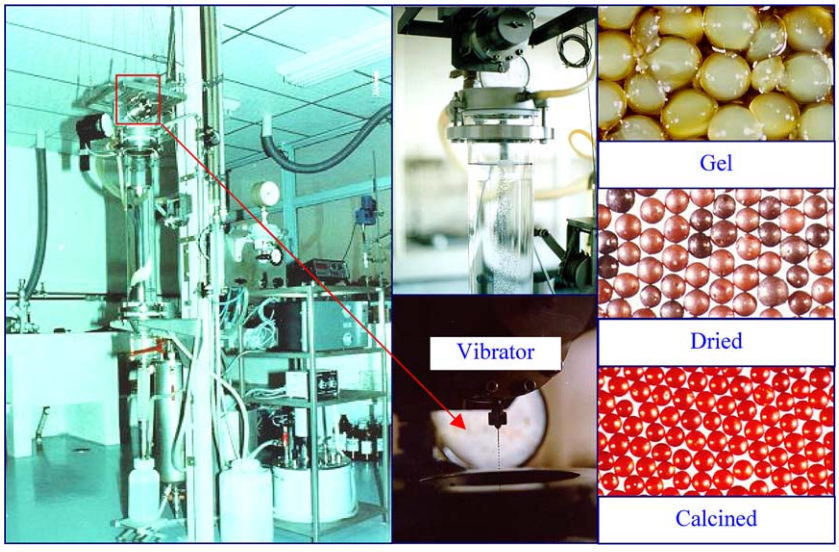

Fig. 1. Production of thorium and uranium kernels.

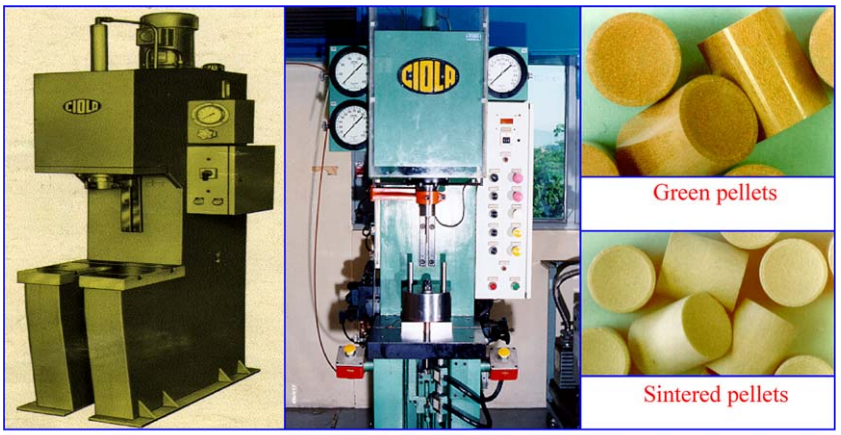

Fig. 2. Hydraulic press for fuel pellets production.

of Argon/4% Hydrogen and at 1700 °C for 2 h. The heating rate was 10 °C/min.

2.3. Kernels compression testing system

Fig. 3 shows the system that was designed to investigate the behavior of one isolated kernel under compression and to measure the kernel crushing strength [6].

The system is composed by two punches and a Plexiglass ring in order to avoid the machine and the laboratory floor contamination by kernels fragments and also in order to allow the observation, film and photograph the kernel under testing.

A universal Instron-TT-DM-L machine with a 500 N CCM ultra-sensitive load cell was used. An upper punch velocity of 0.005 cm/min was used in all tests, and 15 measurements were done for each kernel batch. Fig. 4 shows a typical register of one test.

2.4. Kernel density, diameter and specific surface measurements

A graduate pipette with one extremity obstructed with Teflon® was used to measure the sample volume, and an analytical balance was used to obtain its mass. In order to have a good arrangement of the kernels inside the pipette, the pipette charging with the sample was carried out very slowly and with the aid of two funnels placed in series. By this method, it was obtained the kernels loose bulk density ρ_a. The diameter was measured using a Mitutoyo optical comparator. For the specific surface, it was applied the BET method using an in house made equipment [7].

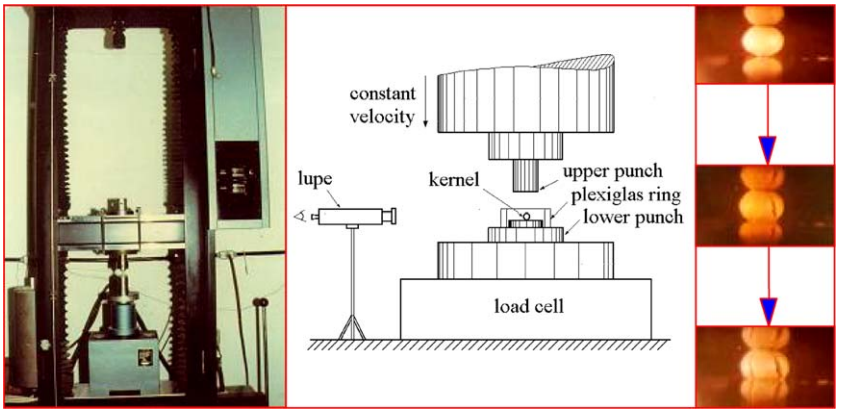

Fig. 3. System to measure the kernels crushing strength.

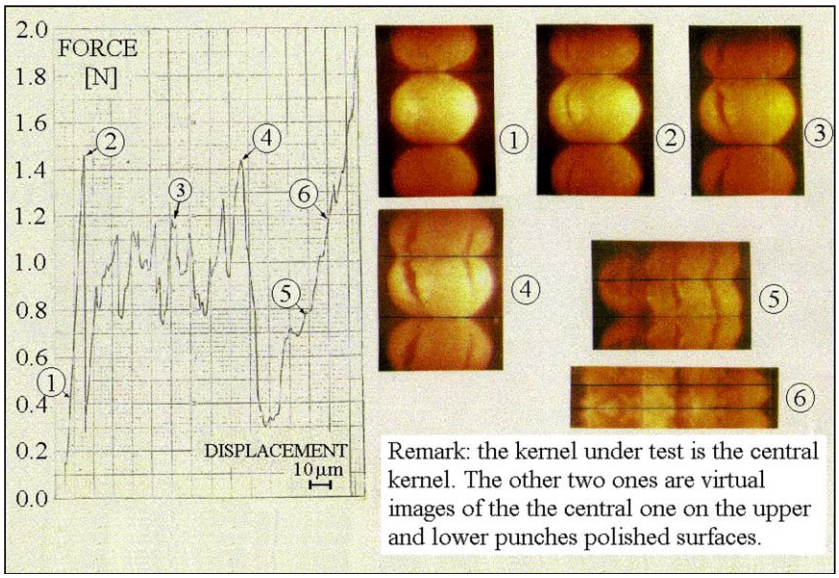

Fig. 4. Typical register of a kernel compression test.

2.5. Kernels and pellets microstructures

The usual metallographic preparation methods and optical and scanning electronic microscopy were used.

2.6. Green pellet density

For the green pellet density determination it was applied a geometrical method consisting of measuring the diameter (d_v) and height (h_v) of the green pellet with a micrometer (resolution 10^{-4} cm), and the mass (m_v) with an analytical balance (resolution 10^{-4} g). The following equation was used:

$$\rho_v = \frac{m_v}{\frac{\pi \cdot d_v^2 \cdot h_v}{4} - 0.031}, \quad (2)$$

where the value 0.031 cm^3 is the volume corresponding to the green pellet dishings and chanfers calculated from the punch dimensions.

2.7. Pellet sintered density and open porosity

It was applied the Penetration-Immersions Method [8–10] developed by Kraftwerk Union that was absorbed and transferred to CDTN.

2.8. Pellet pore and grain size distributions

To reveal the grain structure it was used a thermal attack in CO_2 atmosphere at 600 °C for 2 h. To obtain the grain and pores distributions, it was applied the Saltikov Method [11].

3. Results and discussion

The investigation showed that the kernel behavior is similar to the sol–gel crushed chunks behavior reported in the first historical work taking advantage of sol–gel materials to produce thoria–urania fuel pellets [12]:

- Both the pellets sintered density and the pellet shrinkage decrease with the increase of the kernel calcining temperature and time.
- The apparent strength of the pellet formed from calcined kernels decreased as the calcining temperature increased. This is clearly caused by the increasing of the particles crushing strength when the calcining temperature increases. Consequently, the obtained green pellet has a lower particles mechanical interlock, resulting in a lower apparent strength. In addition, higher particle crushing strength results in a lower closing degree of the voids between the particles and, therefore, in a lower sintered density.
- Green pellets with the same green density, produced with distinct batches, can result in sintered pellets with totally different sintered density. There is not a direct relationship between pellet green density and pellet sintered density with one parameter increasing with the increasing of the other.

Fig. 5 shows the results of the compression tests for 21 kernels batches that were calcined at temperatures that range from 650 °C to 900 °C and different times that range from 3 to 30 h. The characterization results for these groups are presented in Table 1. The kernels diameter of all batches ranges from 270 to 300 μm.

The kernel density increases with the intensity of the calcining (time and temperature) and consequently, the crushing strength increases too. As a result, for a fixed compactation pressure, the sintered density of the corresponding pellet decreases while the kernel density increases, i.e., the higher crushing strength causes an increase in the degree of difficulty to close the voids between the kernels (Fig. 6).

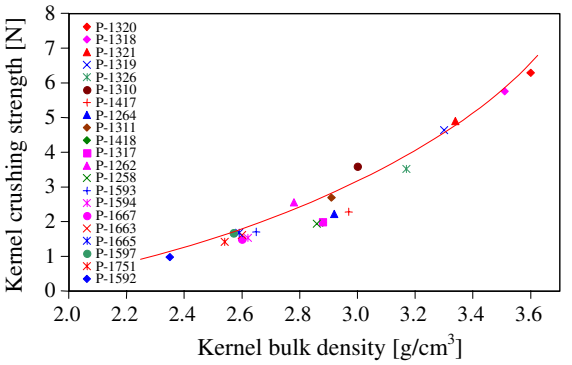

Fig. 5. Increase of the kernel crushing strength with the increasing of its bulk density.

The pellet sintered density decreases due to the large pores presence generated by the voids between the kernels that are not totally closed during pressing, whose dimensions increase with the increasing of the kernel crushing strength.

Fig. 7 displays a typical microstructure of a drastically calcined kernel that has, consequently, a high density and a high crushing strength. In contrast, Fig. 8 shows a very different kernel microstructure that has lower density and lower crushing strength and, consequently, better properties for pelletizing.

The major effort in developing the new fuel production was optimizing the microstructure of the pellet, i.e., to obtain a sintered pellet with a density that satisfies the fuel specified range ($\rho_s = 9.30$–9.65 g/cm^3). At the same time, with a microstructure with total absence of these large pores and the presence of only pores homogeneously distributed that range from 1 to 10 μm. It was clear the necessity to produce kernels with density as low as possible in order to make easier the closing of the voids between the kernels during pressing and, consequently, to obtain pellets with better microstructures. The difficulty was that, if one uses a greater

Table 1
Characterization results of (Th,5%U)O_2 kernels

Batch code	Crushing strength (N)	Bulk density (g/cm^3)	Specific surface (m^2/g)	Calcining temperature and time (°C/h)
P-1320	6.29	3.60	2.5	300/2 + 2 × 900/23
P-1318	5.76	3.51	–	300/2 + 1 × 900/23
P-1321	4.90	3.34	–	300/2 + 2 × 900/23
P-1319	4.63	3.30	–	300/2 + 1 × 900/23
P-1326	3.52	3.17	–	300/2 + 1 × 900/23
P-1310	3.59	3.00	5.1	300/2 + 1 × 900/23
P-1417	2.28	2.97	–	300/2 + 700/20 + 900/3
P-1264	2.22	2.92	–	300/2 + 2 × 700/23
P-1311	2.69	2.91	9.1	300/2 + 700/20 + 900/3
P-1418	1.97	2.88	–	300/2 + 2 × 700/23 + 900/3
P-1317	1.99	2.88	–	300/2 + 2 × 700/23
P-1262	2.55	2.78	–	300/2 + 2 × 700/23 + 900/3
P-1593	1.94	2.86	52.4	650/30
P-1594	1.70	2.65	42.8	650/30
P-1258	1.53	2.62	40.0	300/2 + 2 × 700/23
P-1667	1.49	2.60	22.0	850/3
P-1663	1.61	2.60	24.9	850/3
P-1665	1.67	2.59	22.0	850/3
P-1597	1.67	2.57	21.8	850/3
P-1751	1.42	2.54	31.5	850/3
P-1592	0.97	2.35	31.0	850/3

Carbon black content: 30 g/l.

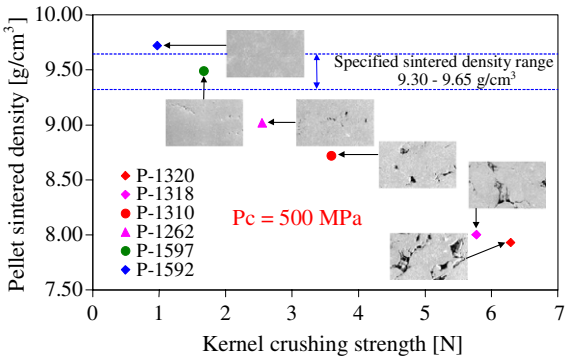

Fig. 6. Influence of the kernel crushing strength on the pellet sintered density and its microstructure.

compactation pressure to close completely the voids between the kernels during pressing, the density of the sintered pellet would be greater than the specified range.

The kernels batches that led to better results were the ones that belonged to the group calcined at 850 °C for 3 h with greater layer thickness of kernels in the calcining boat (2.36, 3.50 and 5.80 mm). The characterization results for this group are summarized in Table 2. The batches of this group calcined with thin bed layer resulted in pellets with improper microstructures due to its higher density and crushing strength.

It was observed a strong influence of the kernels bed layer thickness on their properties. It was found a density and a specific surface gradient along the kernels bed layer that caused a loss of homogeneity in the pellet pore distribution. This effect led to design a rotating kiln to the kernels calcining and the problem was solved.

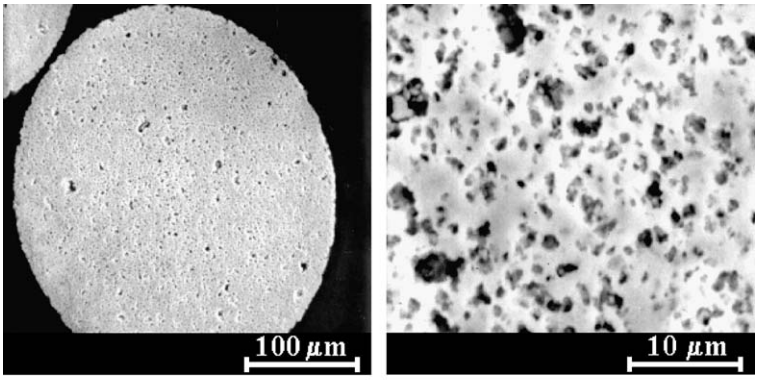

$\rho_a = 3.60$ g/cm^3 $F_c = 6.29$ N $S_g = 2.5$ m^2/g

Fig. 7. Microstructure of a kernel with higher bulk density and higher crushing strength.

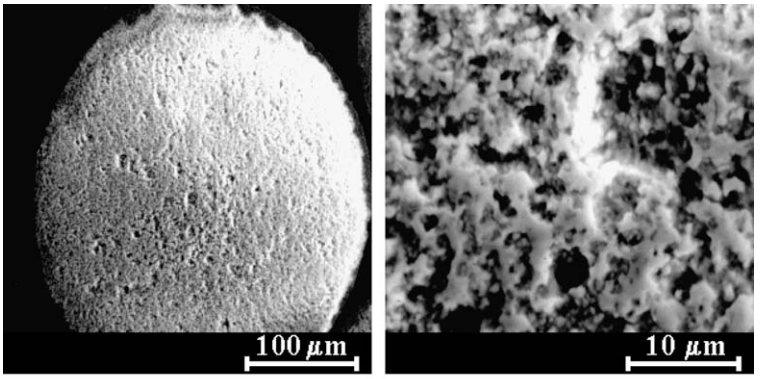

$\rho_a = 2.60$ g/cm^3 $F_c = 1.61$ N $S_g = 29.9$ m^2/g

Fig. 8. A kernel microstructure with lower bulk density and lower crushing strength.

Table 2
Characterization data of (Th,5%U)O_2 kernels calcined at 850 °C per 3 h with different kernel layers thickness in the calcining boat

Batch code	Crushing strength (N)	Bulk density (g/cm^3)	Specific surface (m^2/g)	Layer thickness (mm)
P-1894	1.17	2.33	29.0	5.80
P-1592	0.97	2.35	31.0	5.80
P-1901	1.05	2.38	32.4	5.80
P-1909	1.20	2.43	22.6	3.50
P-1897	1.14	2.44	26.4	5.80
P-1910	1.32	2.45	22.1	2.36
P-1914	1.20	2.49	22.2	3.50
P-1895	1.45	2.51	21.9	1.21
P-1597	1.67	2.57	21.8	4.00
P-1900	1.56	2.58	24.2	1.21
P-1995	1.44	2.59	24.1	2.70
P-1665	1.67	2.59	22.0	4.00
P-1663	1.61	2.60	24.9	4.00
P-1667	1.49	2.60	22.0	4.00
P-1948	1.50	2.60	21.1	2.70
P-1904	0.99	2.61	21.2	5.80
P-1991	1.58	2.62	23.6	2.70
P-1952	1.39	2.63	22.7	2.70
P-1989	1.87	2.63	23.1	2.70
P-1955	1.59	2.64	21.9	2.70
P-1896	1.54	2.65	21.9	1.21
P-1907	1.14	2.65	22.3	5.80
P-2031	1.64	2.65	22.6	2.70
P-1980	1.55	2.65	23.4	2.70
P-1916	1.41	2.72	16.1	2.36
P-1999	1.83	2.73	23.0	2.70
P-2018	1.60	2.73	23.0	2.70
P-1911	1.87	2.74	20.0	0.36
P-1918	1.40	2.75	17.9	0.36
P-2015	1.63	2.75	20.0	2.70
P-2016	1.51	2.75	22.3	2.70
P-2017	1.61	2.75	22.4	2.70
P-2005	1.60	2.77	22.1	2.70
P-2012	1.77	2.78	22.3	2.70
P-1913	1.80	2.81	22.8	0.36
P-1906	1.71	2.83	19.5	1.21
P-1903	1.73	2.84	15.6	1.21
P-1917	2.06	3.03	17.8	0.36
P-1915	2.09	3.07	16.5	0.36

Carbon black content: 30 g/l.

It was possible to obtain a pellet with 9.50 g/cm^3 sintered density with a reduced quantity of large pores with batches that are calcined at 850 °C for 3 h with the largest used bed layer thickness, but it needed an optimization of its microstructure.

A comparison between the pelletizing results of this group and the results of the two batches that were calcined at 650 °C, indicated the way to optimize the microstructure. These two batches had greater specific surface related to the group calcined at 850 °C. As a result, they needed a relatively lower compactation pressure to reach the specified pellet sintered density because of its higher sintering activity. Consequently, the microstructures of the corresponding pellets have a relatively greater quantity of large pores and higher open porosity. It is the worst case (Fig. 9).

It was concluded the necessity to produce kernels with lower specific surface simultaneously with lower density. The idea was compensating a lower sintering activity caused by a lower specific surface through a relatively higher compactation pressure that enables a total closing of the voids between the kernels without exceeding the specified sintered density range ($\rho_s = 9.30$–9.65 g/cm^3).

It was necessary to increase the calcining temperature in order to obtain kernels with lower specific surface. But an increase in the calcining temperature would cause a harmfull increase in the kernel density. The way to solve this problem was by compensating for the higher temperature through an increase in the pore former quantity. Several batches were produced with higher carbon black content (38, 45 and 60 g/l) and calcined at higher temperatures that range from 950 °C to 1000 °C. Kernels with simultaneously lower density and specific surface were obtained, the model was confirmed and the fuel pellet microstructure was optimized (Fig. 10). The characterization results for this group are presented in Table 3.

Fig. 11 displays the influence of the specific surface on the fuel pellet open porosity. Only kernels with lower specific surface result in pellets with open porosity according to the fuel specification (open porosity < 1 vol.%).

The average grain size of all pellets was approximately 15 μm independently of the kernels properties (Fig. 12), and according to the fuel specification.

3.1. Mathematical model

As the kernel crushing strength is a function of the kernel density, Eq. (1) can be simplified. The sintered density can be expressed only as a function of the density, specific surface and compactation pressure:

$$\rho_s = \rho_s(\rho_m, S_g, P_c). \quad (3)$$

For the group calcined at 850 °C for 3 h, the sintered density can be expressed independently of the specific surface because the corresponding specific surface values were situated in a relatively

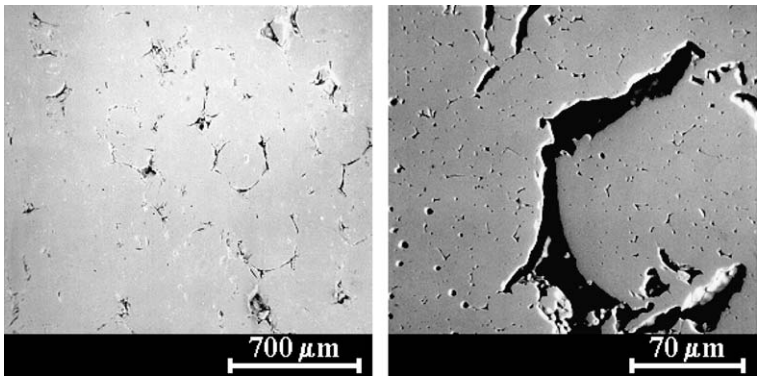

Fig. 9. Pellet microstructure obtained from kernels calcined at 650 °C.

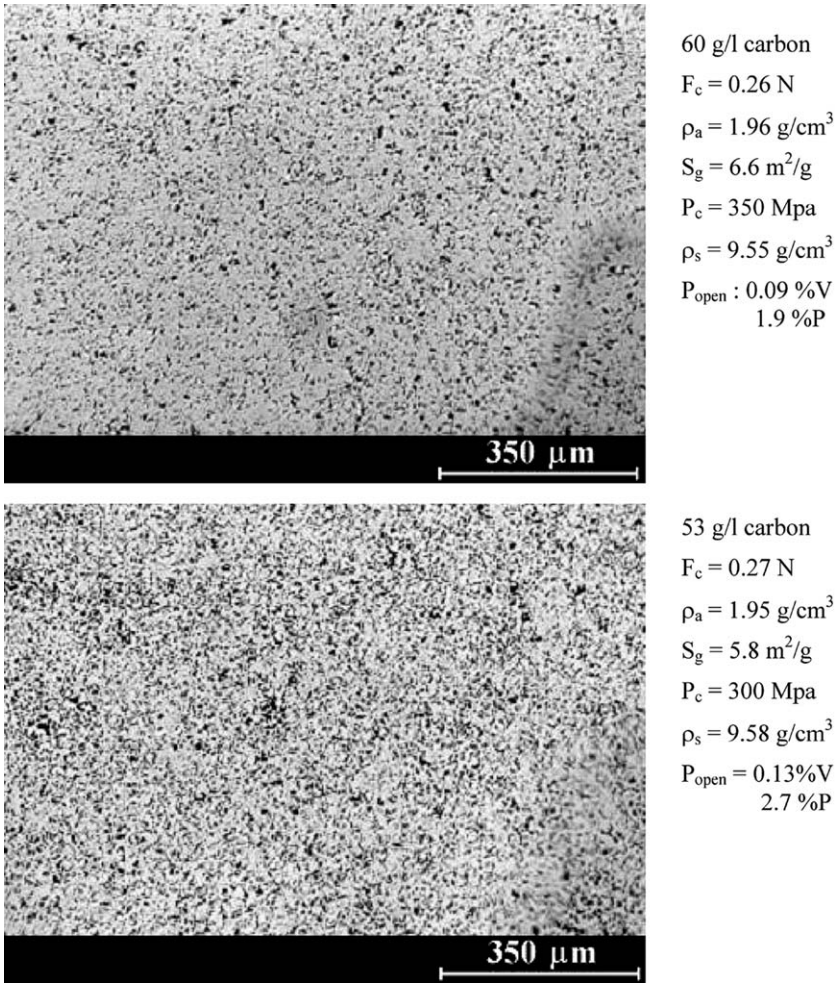

Fig. 10. Optimized (Th,5%U)O_2 fuel pellet microstructure.

narrow range (15.6–32.4 m^2/g). For this group, a restricted model according to Fig. 13 was created with the kernels loose bulk density (ρ_a) instead of the kernels density (ρ_m), i.e.,

Table 3
Characterization results of batches produced with higher content of carbon black and calcined at temperatures that range from 850 °C to 1000 °C

Batch code	Carbon black (g/l)	Calcining temperature/time (°C/h)	Crushing strength (N)	Bulk density (g/cm^3)	Specific surface (m^2/g)
P-2043	38	850/3	0.96	2.35	24.9
P-2044	38	900/3	1.33	2.46	10.3
P-2045	38	920/2	1.63	2.51	8.6
P-2127-A	38	930/1	1.00	2.41	9.6
P-2127-B	38	920/2	0.85	2.41	15.7
P-2127-C	38	920/3	0.93	2.36	10.2
P-2127-D	38	920/3	1.22	2.55	10.9
P-2128-A	38	930/1	0.95	2.37	13.5
P-2128-B	38	920/2	1.35	2.55	13.4
P-2128-C	38	920/2	0.79	2.30	15.2
P-2128-D	38	990/0:20	0.78	2.40	20.2
P-2139-A	38	950/2	1.18	2.49	7.5
P-2139-B	38	950/1	1.21	2.60	7.7
P-2139-C	38	950/1	1.09	2.56	8.4
P-2139-D	38	950/2	0.75	2.42	14.6
P-2140-D	38	950/2	1.00	2.40	–
P-2134-A	45	1.000/1	0.71	2.33	5.6
P-2134-B	45	980/2	1.12	2.58	3.5
P-2135	38	950/2	0.90	2.38	10.4
P-2136	38	950/2	0.88	2.42	9.6
P-2137	38	950/2	0.90	2.44	9.8
P-2138	38	950/2	0.79	2.44	9.8
P-2140	38	950/2	0.99	2.41	9.4
P-2163-B	38	950/2 Rotating camera	1.00	2.68	5.1
P-2166-C	45	950/2 Rotating camera	0.34	2.27	5.1
P-2164-B	53	950/2 Rotating camera	0.25	2.06	5.4
P-2165-C	60	950/2 Rotating camera	–	1.83	7.1
P-2163-A	38	950/2 Rotating camera	0.91	2.48	5.0
P-2166-B	45	950/2 Rotating camera	0.48	2.20	5.8
P-2164-A	53	950/2 Rotating camera	0.27	1.95	5.8
P-2165-A	60	950/2 Rotating camera	0.14	1.74	5.6
P-2166-A	45	950/2 Rotating camera	0.76	2.35	6.2
P-2165-B	60	950/2 Rotating camera	0.26	1.96	6.6
P-2171-B	45	950/2 Rotating camera	–	2.50	6.4
P-2171-C	45	950/2 Rotating camera	–	2.50	6.0
P-2171-D	45	950/2 Rotating camera	0.60	2.35	6.7
P-2171-E	45	950/2 Rotating camera	–	2.53	6.1
P-2171-F	45	950/2 Rotating camera	–	2.37	7.0

$$\rho_s = \rho_s(\rho_a, P_c). \quad (4)$$

The difference between the (Th,5%U)O_2 theoretical density (straight dashed line in Fig. 13) and the pellet sintered density (curve line) can be fitted as a function of the kernels bulk density by an exponential law:

$$\ln(\rho_{th} - \rho_s) = a \cdot \rho_a + b, \quad (5)$$

$$\therefore \rho_s = \rho_{th} - \exp[a \cdot \rho_a + b]. \quad (6)$$

This relation was chosen because in the investigated range the experimental data fit reasonably well to the exponential law. There is not a physical reason for that choice. The same is applied to Eq. (15).

By the minimum square method, it was obtained for each compactation pressure, the values for a and b shown in Table 4.

By the same method, it was obtained the following expressions for a and b:

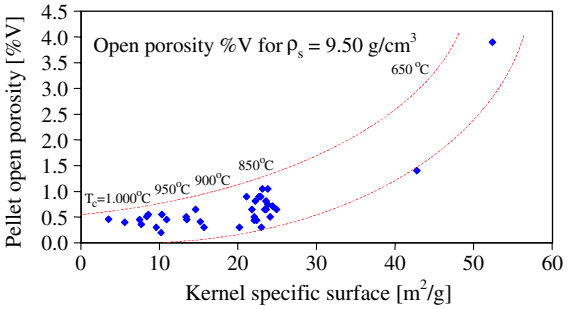

Fig. 11. Fuel pellet open porosity as a function of the kernel specific surface.

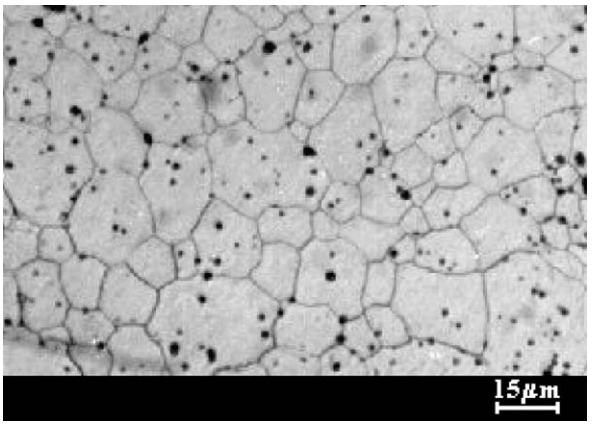

Fig. 12. Typical grain structure of (Th,5%U)O_2 fuel pellets.

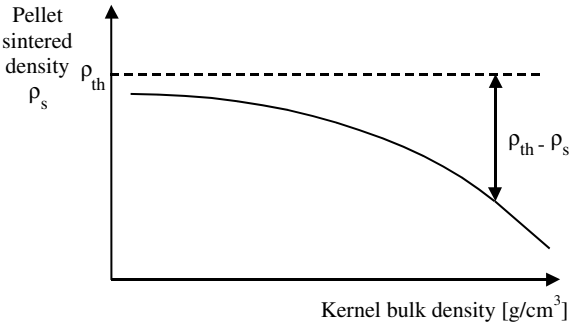

Fig. 13. Increase of the difference between the theoretical density and the pellet sintered density with the increasing of the kernel bulk density.

$$a = 0.329 \ln P_c - 0.832 \quad (r = 0.97), \tag{7}$$

$$b = -1.759 \ln P_c + 7.081 \quad (r = 0.99). \tag{8}$$

Substituting a and b in Eq. (6), it was obtained the following mathematical expression for Eq. (4):

Table 4
Result of Eq. (6) adjustment

Compactation pressure (MPa)	a (cm^3/g)	b (dimensionless)	Correlation factor
300	1.021	−2.893	0.96
400	1.161	−3.507	0.94
500	1.231	−3.897	0.95
600	1.289	−4.210	0.95
700	1.293	−4.364	0.95

$$\rho_s = \rho_{th} - \exp[(0.329 \ln P_c - 0.832).\rho_a - 1.759 \ln P_c + 7.081] \quad (g/cm^3). \tag{9}$$

Fig. 14 shows the curves corresponding to this equation for several values of the compactation pressure. From Eq. (9),

$$P_c = \exp\left[\frac{\ln(\rho_{th} - \rho_s) + 0.832.\rho_a - 7.081}{0.329.\rho_a - 1.759}\right]. \tag{10}$$

By this equation, it is possible to calculate the necessary compactation pressure to produce pellets with a determined sintered density ρ_s with kernels calcined at 850 °C for 3 h and that has a determined bulk density ρ_a.

Introducing in Eq. (10) $\rho_{th} = 10.05$ g/cm^3 for the (Th,5%U)O_2 fuel and ρ_s equals to the specified sintered density for this fuel ($\rho_s = 9.50$ g/cm^3), one obtains the following equation for the optimal compactation pressure P_{co}^{850} for this group calcined at 850 °C for 3 h:

$$P_{co}^{850} = \exp\left(\frac{0.832 \cdot \rho_a - 7.679}{0.329 \cdot \rho_a - 1.759}\right). \tag{11}$$

This equation fits very well to the optimal compactation pressure values extracted from 39 characteristic curves ($\chi^2 = 1.37$), and it was an efficient tool for the pelletizing experiments.

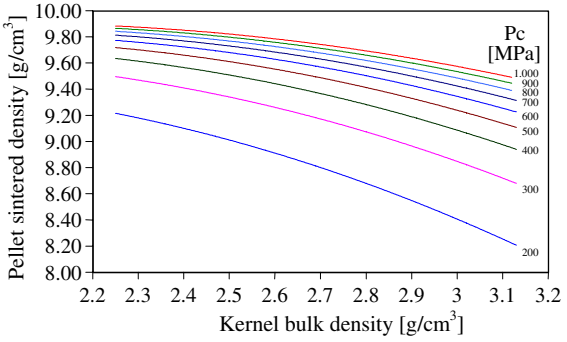

Fig. 14. Curves of the pellet sintered density as a function of the kernel bulk density.

Generalizing the restricted model, the group calcined at 850 °C was taken as reference. The corresponding values of the optimal compactation pressure were compared to the values of other batches that have relatively lower and higher specific surfaces, due to the higher and the lower calcining temperature, respectively. The concept of ΔP_{co} was created, dependent on the kernel specific surface, as being the compactation pressure value to be added or subtracted from the value calculated by Eq. (11), to compensate a higher or lower sintering activity caused by a higher or lower specific surface:

$$\Delta P_{co} = \Delta P_{co}(S_g). \tag{12}$$

In a general case, the compactation pressure will be

$$P_{co} = P_{co}^{850} + \Delta P_{co}(S_g). \tag{13}$$

The respective value of ΔP_{co} was calculated for each batch, positive or negative, which is the difference between the optimal compactation pressure P_{co} of each batch, extracted from the respective characteristic curve, and the value calculated by Eq. (11):

$$\Delta P_{co} = P_{co} - P_{co}^{850}. \tag{14}$$

Fig. 15 shows the obtained result. A referential change was made in order to use positive values and continue to use the logarithmical function. It was chosen as reference the value 250 MPa in the scale of ΔP_{co}, because this value is above all the observed ones.

By the minimum square method, the data was adjusted to the following equation:

$$\ln(250 - \Delta P_{co}) = a \cdot S_g + b. \tag{15}$$

The following values were obtained for a and b:

$a = 0.02$,

$b = 5.1$.

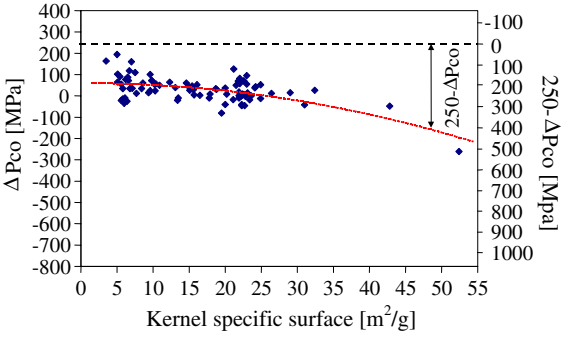

Fig. 15. Kernel specific surface influence on ΔP_{co}.

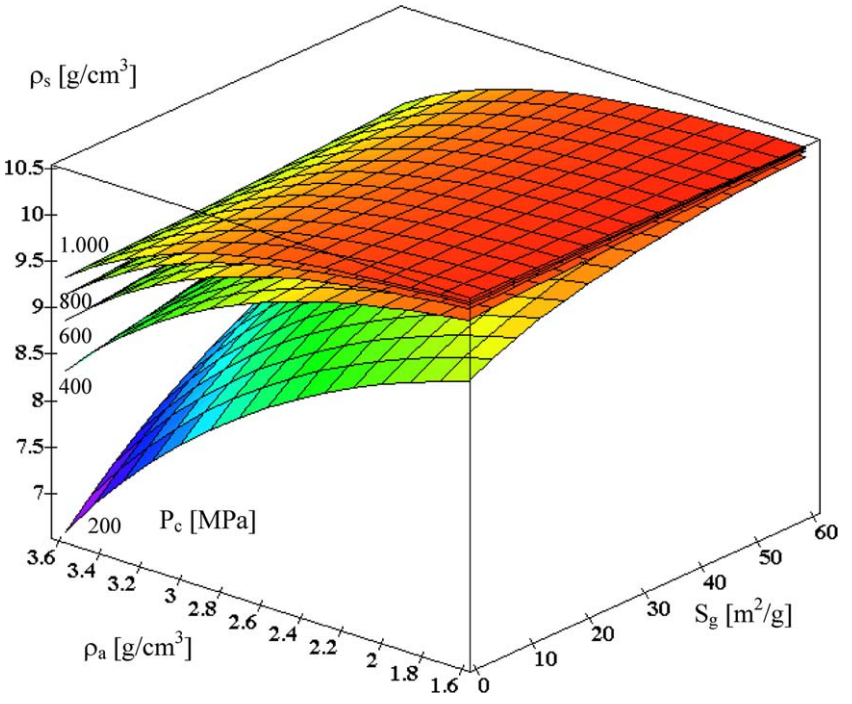

Fig. 16. Surfaces corresponding to Eq. (20).

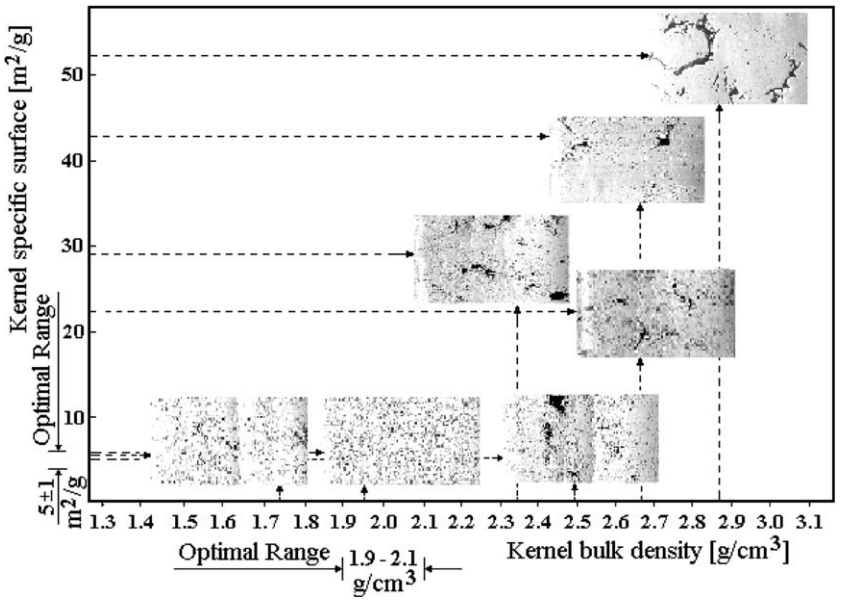

Fig. 17. $(Th,5\%U)O_2$ fuel pellets, all with density in the specified range, but with different pore structures as a function of the kernels properties, bulk density and specific surface.

Substituting a and b in Eq. (15), it was obtained the following expression for ΔP_{co}:

$$\Delta P_{co} = 250 - \exp(0.02.S_g + 5.1). \quad (16)$$

Substituting in Eq. (13),

$$P_{co} = P_{co}^{850} - \exp(0.02.S_g + 5.1) + 250. \quad (17)$$

Introducing the value of P_{co}^{850} from Eq. (11), it was obtained the following:

$$P_{co} = \exp\left(\frac{0.832 \cdot \rho_a - 7.679}{0.329 \cdot \rho_a - 1.759}\right) - \exp(0.02 \cdot S_g + 5.1) + 250. \quad (18)$$

This expression allows to calculate accurately, in order to satisfy the fuel specification, the optimal compactation pressures for kernels that have a determined bulk density ρ_a, and a determined specific surface S_g.

In a general case one has

$$P_c = \exp\left[\frac{\ln(\rho_{th} - \rho_s) + 0.832.\rho_a - 7.679}{0.329.\rho_a - 1.759}\right] - \exp(0.02.S_g + 5.1) + 250. \quad (19)$$

After isolating ρ_s, the following expression for the general equation (1) is obtained:

$$\rho_s = \rho_{th} - \exp\{\{0.329\ln[P_c - 250 + \exp(0.02 \cdot S_g + 5.1)] - 0.832\} \cdot \rho_a - 1.759\ln[P_c - 250 + \exp(0.02S_g + 5.1)] + 7.081\}. \quad (20)$$

Fig. 16 displays the surfaces corresponding to Eq. (20) and Fig. 17 sintetizes the interralations between the kernels properties and the fuel sintered pellet microstructures.

4. Conclusion

It was possible, with the developed methods and appropriate equipments, to measure the kernel properties, produce nuclear fuel pellets, reveal the kernel behavior in the pelletizing process and optimize the microstructure of the new fuel. A very efficient tool to preview the properties, density and microstructure of the fuel pellet was established by a mathematical expression. It allows to calculate the sintered density that will be obtained in the pellet, as a function of the kernels properties, density and specific surface. One intends to test this method with another types of sol–gel spherical fissile materials because one believes that it can be applied to any type of spherical particles used for pellets fabrication through powder metallurgy techniques.

References

[1] KFA, KWU/SIEMENS, NUKEM, NUCLEBRÁS/CDTN, Program of research and development on the thorium utilization in PWRS – Final Report, Kernforschungsanlage Jülich GmbH, Jülich, 1988, 235 p. (Jül-Spez. 488).

[2] M. Peehs, W.O. Dörr, H. Hrovat, et al., in: IAEA Advisory Group Meeting on Advanced Fuel Technology and Performance, 1984, Wuerenlingen, Switzerland/IAEA, Vienna, 1985, 244 p., p. 175 (IAEA-TECDOC-352/85).
[3] M. Kadner, J. Baier, Kerntechnik 18 (10) (1976) 413.
[4] P. Naefe, Beitrag zur Refabrikation von Th/U – Mischoxidkernen mit einen naßchemischen Verfaheren, Kernforschungsanlage Jülich GmbH, Jülich, 1975, 78 p. (Jül-1229).
[5] R.A.N. Ferreira, Projeto de sistema para compactação de pastilhas combustíveis, NUCLEBRÁS/CDTN, Belo Horizonte, 1979, 11 p. (Technical Report DITCO.PD.004/79).
[6] R.A.N. Ferreira, Comportamento de microesferas de (Th,5%U)O_2 em ensaios de compressão e peletização, Escola de Engenharia da Universidade Federal de Minas Gerais, Belo Horizonte, 1982, 92 p. (MSc Dissertation in Science and Nuclear Techniques).
[7] R.A.N. Ferreira, O. Miranda, S.C. Reis, et al., in: 34° Congresso Brasileiro de Cerâmica, 1990, Associação Brasileira de Cerâmica, São Paulo, Blumenau, Santa Catarina, 1990, p. 530.
[8] W. Dörr, H. Assmann, G. Maier, J. Steven, J. Nucl. Mater. 81 (1979) 135.
[9] G. Maier, Dichte und Porositätsmessung nach der Penetrations-Imersions Methode: Überprüfung und Möglichkeiten zur Verbesserung, Kraftwerk Union, Erlangen, 1978, 22 p. (Arbeits-Bericht).
[10] G. Maier, Round Robin – Dichtmeß – Programm, Abschließende Ergebnisse, Kraftwerk Union, Erlangen, 1976, 13 p. (Ergebnis-Bericht).
[11] S.A. Saltikov, Stereometrische Metallographie, VEB, Leipzig, 1974.
[12] J.M. Robbins, J.G. Stradley, Fabrication of sol–gel-derived thoria–urania by cold pressing and sintering, Oak Ridge National Laboratory, ORNL-4426, Paper presented at the Sixty-Ninth Annual Meeting, The American Ceramic Society, New York City, 2 May 1967.